JACS
JOURNAL OF THE AMERICAN CHEMICAL SOCIETY
Article
pubs.acs.org/JACS

Magic Ratios for Connectivity-Driven Electrical Conductance of Graphene-like Molecules

Yan Geng,[†,§] Sara Sangtarash,*[,‡,§] Cancan Huang,[†,§] Hatef Sadeghi,[‡,§] Yongchun Fu,[†] Wenjing Hong,*[,†] Thomas Wandlowski,[†] Silvio Decurtins,[†] Colin J. Lambert,*[,‡] and Shi-Xia Liu*[,†]

[†]Department of Chemistry and Biochemistry, University of Bern, Freiestrasse 3, CH-3012 Bern, Switzerland
[‡]Lancaster Quantum Technology Centre, Department of Physics, Lancaster University, Lancaster LA1 4YB, U.K.

Supporting Information

ABSTRACT: Experiments using a mechanically controlled break junction and calculations based on density functional theory demonstrate a new magic ratio rule (MRR) that captures the contribution of connectivity to the electrical conductance of graphene-like aromatic molecules. When one electrode is connected to a site i and the other is connected to a site i' of a particular molecule, we assign the molecule a "magic integer" $M_{ii'}$. Two molecules with the same aromatic core but different pairs of electrode connection sites (i,i' and j,j', respectively) possess different magic integers $M_{ii'}$ and $M_{jj'}$. On the basis of connectivity alone, we predict that when the coupling to electrodes is weak and the Fermi energy of the electrodes lies close to the center of the HOMO−LUMO gap, the ratio of their conductances is equal to $(M_{ii'}/M_{jj'})^2$. The MRR is exact for a tight-binding representation of a molecule and a qualitative guide for real molecules.

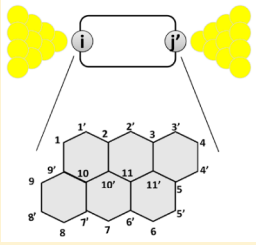

	1′	2′	3′	4′	5′	6′	7′	8′	9′	10′	11′
1	-9	7	-4	4	-1	1	-1	1	-1	2	-3
2	-1	-7	4	-4	1	-1	1	-1	1	-2	3
3	1	-3	-4	4	-1	1	-1	1	-1	2	-3
4	-1	3	-6	-4	1	-1	1	-1	1	-2	3
5	1	-3	6	-6	-1	1	-1	1	-1	2	-3
6	-1	3	-6	6	-9	-1	1	-1	1	-2	3
7	3	-9	8	-8	7	-7	-3	3	-3	6	1
8	-6	8	-6	6	-4	4	-4	-6	6	-2	-2
9	6	-8	6	-6	4	-4	4	-4	-6	2	2
10	3	1	-2	2	-3	3	-3	3	-3	-4	1
11	-2	6	-2	2	2	-2	2	-2	2	-4	-4

INTRODUCTION

Charge transport through polycyclic aromatic hydrocarbons (PAHs) has attracted intensive attention in recent years,[1,2] partly because of their role in the design and development of molecular electronic devices.[3−6] Since PAHs are well-defined and defect-free, they also provide model systems for understanding transport in graphene (treated as an infinite alternant PAH) and graphene-based nanostructures.[7−9] When a single molecule is connected to metallic electrodes, electrons passing through the molecule from one electrode to the other can remain phase-coherent, even at room temperature.[10,11] This has led to a great deal of discussion about the role of quantum interference (QI) in determining the electrical conductance of single molecules,[12−21] culminating in a series of recent experiments revealing room-temperature signatures of QI.[22−30]

Both experiment and theory have focused primarily on elucidating the conditions for the appearance of constructive or destructive interference. In the simplest case, where electrons are injected at the Fermi energy (E_F) of the electrodes, constructive QI arises when E_F coincides with a delocalized energy level of the molecule (E_n). Similarly, a simple form of destructive QI occurs when E_F coincides with the energy of a bound state located on a pendant moiety (E_b).[31,32] In practice, unless the energy levels are tuned by electrostatic, electrochemical, or mechanical gating, molecules located within a junction rarely exhibit these types of QI because E_F is usually located in the HOMO−LUMO (H−L) gap. For this reason, discussions have often focused on conditions for destructive or constructive QI when E_F is located at the center of the H−L gap. For the purpose of identifying conditions for destructive QI within the delocalized π system, a useful conceptual approach is to represent molecules by lattices of connected sites (C(sp^2) atoms), such as those shown in Figure 1, in which (a) represents a benzene ring, (b) represents naphthalene, (c) represents anthracene, and (d) represents anthanthrene. Such abstractions highlight the role of connectivity in determining the presence or absence of destructive QI. For example, the lattices of Figure 1 are bipartite, being composed of equal numbers of "primed" and "unprimed" sites, such that primed sites (labeled by primed integers, e.g., 1′, 2′, 3′) are connected only to unprimed sites (labeled by nonprimed integers, e.g., 1, 2, 3) and vice versa. It is well-known[33−38] (see Mathematical Methods below) that if electrodes are connected to two sites that are both primed or both unprimed, then destructive interference occurs and the contribution from the π orbitals to the electrical conductance (G) vanishes. For a phenyl ring, this corresponds to the well-known case of meta-coupled electrodes,[31] but more generally it holds for any bipartite lattice.

Studies of such lattices have yielded a variety of simple rules for the appearance of destructive QI,[21,32−37] for which the π-orbital contribution to G vanishes. The aim of the present paper is to elucidate a simple rule for determining the nonzero values of electrical conductance arising from constructive QI in aromatic molecules. At first sight, this task seems rather daunting, because there is only one conductance (i.e., $G = 0$) when QI is destructive, whereas there are many possible nonzero values of G when QI is constructive. Furthermore, the

Received: January 12, 2015
Published: March 17, 2015

DOI: 10.1021/jacs.5b00335
J. Am. Chem. Soc. 2015, 137, 4469−4476

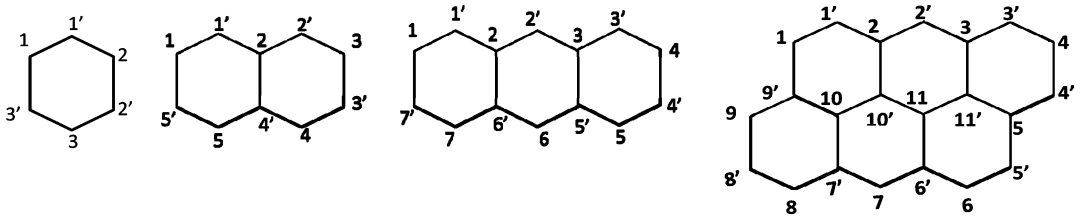

Figure 1. Four examples of bipartite lattices, with the magnitudes of their magic numbers shown underneath each lattice: (a) benzene, (b) naphthalene, (c) anthracene, and (d) anthanthrene.

nonzero values of the conductance in the presence of constructive QI depend on the strength and detailed nature of the contacts to the electrodes.

Remarkably, in what follows we demonstrate a "magic ratio rule" (MRR) based on tables of quantum numbers $M_{ii'}$ that capture the contribution of connectivity to the electrical conductance of graphene-like aromatic molecules, or molecules with graphene-like cores, when one electrode is connected to an "unprimed" site i and the other is connected to a "primed" site i'. In particle physics, quantum numbers such as "charm" and "color" are assigned to elementary particles. In the case of lattices such as those in Figure 1, we refer to these new quantum numbers $M_{ii'}$ as "magic integers" (MIs). For each of the molecules shown in Figure 1, the allowed values of $|M_{ii'}|$ are shown beneath each lattice. Clearly, the spectrum of MIs increases with the size of the aromatic core. The precise values of $M_{ii'}$ are not trivial, since for example $M_{ii'} = 5$ is missing from the set of anthanthrene MIs.

RESULTS AND DISCUSSION

MIs capture the complexity of interference patterns created by electrons at the center of the H−L gap and allow the prediction of conductance ratios via the MRR, which states that "the ratio of conductances of two molecules is equal to the square of the ratio of their magic integers." Clearly, when comparing conductances of the same aromatic core but different contacts, the signs of the MIs are irrelevant. This rule is derived in Mathematical Methods. To each lattice such as those in Figure 1, the quantum numbers $M_{ii'}$ form a table of MIs, which we call an M-table. As shown in the Supporting Information (SI), for the benzene ring (Figure 1a) this is a 3 × 3 table with all of the entries equal to ±1, so $|M_{ii'}| = 1$ is the only possibility. Therefore, as expected, para (i.e., 3,1′) or ortho (3,2′ or 3,3′) connectivities yield the same electrical conductances. For the naphthalene lattice (Figure 1b), the 5 × 5 M-table is shown in Table 1. As expected from symmetry, this table shows that the conductances associated with contact sites 1,1′ and 5,5′ are equal and proportional to $(2)^2 = 4$. It also shows that the conductance with contact sites 4,2′ or 4,3′ would have the same value, which is a less obvious result.

The MRR is an exact formula for conductance ratios of tight-binding representations of molecules in the weak-coupling limit, when the Fermi energy is located at the center of the H−L gap. It does not depend on the size of the H−L gap and is independent of asymmetries in the contacts. In what follows, we explore the real-life implications of the MRR by evaluating the conductance ratio of two molecules both experimentally and using density functional theory (DFT) combined with nonequilibrium Green's functions (NEGF).

Table 1. M-Table of MIs $M_{ii'}$ for the Naphthalene Lattice in Figure 1b[a]

	1′	2′	3′	4′	5′
1	-2	1	-1	1	-1
2	-1	-1	1	-1	1
3	1	-2	-1	1	-1
4	-1	2	-2	-1	1
5	2	-1	1	-1	-2

[a]It should be noted that in all of the M-tables, the first (row) index is unprimed and the second (column) index is primed.

To aid the experimental investigation of the MRR, it is helpful to select two molecules exhibiting constructive QI with very different values of $M_{ii'}$, and therefore, on the basis of the M-table shown in Table 2, we compared the conductance of

Table 2. M-Table for the Anthanthrene Lattice in Figure 1d

	1′	2′	3′	4′	5′	6′	7′	8′	9′	10′	11′
1	-9	7	-4	4	-1	1	-1	1	-1	2	-3
2	-1	-7	4	-4	1	-1	1	-1	1	-2	3
3	1	-3	-4	4	-1	1	-1	1	-1	2	-3
4	-1	3	-6	-4	1	-1	1	-1	1	-2	3
5	1	-3	6	-6	-1	1	-1	1	-1	2	-3
6	-1	3	-6	6	-9	-1	1	-1	1	-2	3
7	3	-9	8	-8	7	-7	-3	3	-3	6	1
8	-6	8	-6	6	-4	4	-4	-6	6	-2	-2
9	6	-8	6	-6	4	-4	4	-4	-6	2	2
10	3	1	-2	2	-3	3	-3	3	-3	-4	1
11	-2	6	-2	2	2	-2	2	-2	2	-4	-4

molecule **1**, derived from an anthanthrene core as shown in Scheme 1 and having an MI of $M_{15'} = -1$, with that of the corresponding molecule **2**, for which $M_{72'} = -9$. Thus, the MRR prediction is that the electrical conductance of the core of **2** should be $(9)^2 = 81$ times higher than that of the core of **1**. Below we demonstrate that even though **1** and **2** differ from the idealization of Figure 1d, this ratio is reflected in mechanically controllable break junction (MCBJ) measurements of their

DOI: 10.1021/jacs.5b00335
J. Am. Chem. Soc. 2015, 137, 4469−4476

Scheme 1. Structures of the Two Molecules Studied Experimentally, Each with the Anthanthrene Core; Following the Numbering Convention in Figure 1d, 1 is Long-Axis-Contacted with Connection Sites 1,5′ and 2 is Short-Axis-Contacted with Connection Sites 7,2′

1 R = -OC_8H_{17}

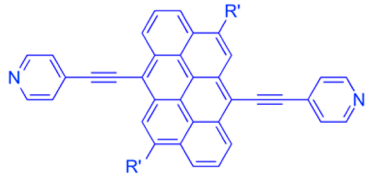

2 R' = 4-(2-ethylhexyloxy)phenyl

conductances, which reveal that the single-molecule conductance of short-axis-contacted anthanthrene **2** is approximately 79 times higher than that of its long-axis-contacted analogue **1**.

Anthanthrene is the compact dibenzo[*def*,*mno*]chrysene molecule, which, together with its angular counterpart dibenzo[*b*,*def*]chrysene, represents a promising building block for many applications in the field of organic electronic materials.[39−41] Advantageously, what sets these prototypical nonlinear PAHs apart from the linearly fused acenes, such as anthracene and pentacene, is the enhanced stability toward degradative chemical reactions and photooxidation.[42−44] The synthetic approach to the two novel pyridine-terminated anthanthrene derivatives **1** and **2** shown in Scheme 1 is reported in the SI. To measure their single-molecule electrical conductances, we employed an MCBJ setup capable of operating in solution. In an MCBJ experiment, molecular junctions are formed by opening and closing a nanogap between two gold electrodes. For further details of conductance measurements, the reader is referred to our previous publications.[22,45,46]

Figure 2a displays typical conductance (G) versus distance (Δz) stretching traces (plotted on a semilogarithmic scale) recorded for 0.1 mM **1** and **2** in a solution of mesitylene and THF (4:1 v/v) using the MCBJ technique. For reference, we have also plotted two traces representing the molecule-free solution (black curves), which reveal classical tunneling characteristics, i.e., an exponential decrease in the conductance upon junction elongation. After the Au−Au contacts break, the formation of molecular junctions is signaled by the presence of additional plateaus in the range $10^{-3}G_0 \geq G \geq 10^{-7.0}G_0$ (where $G_0 = 2e^2/h$ is the quantum of conductance). Typically 1000 individual G versus Δz traces were recorded for both **1** and **2** and analyzed further by constructing all-data-point histograms without any data selection (as shown in Figure 2b) to extract statistically significant results from the different junction configurations. The prominent peaks between $10^{-7}G_0$ and $10^{-4}G_0$ represent molecular junction features. The statistically most probable conductance of each molecular junction is obtained by fitting Gaussians to the characteristic maxima in the

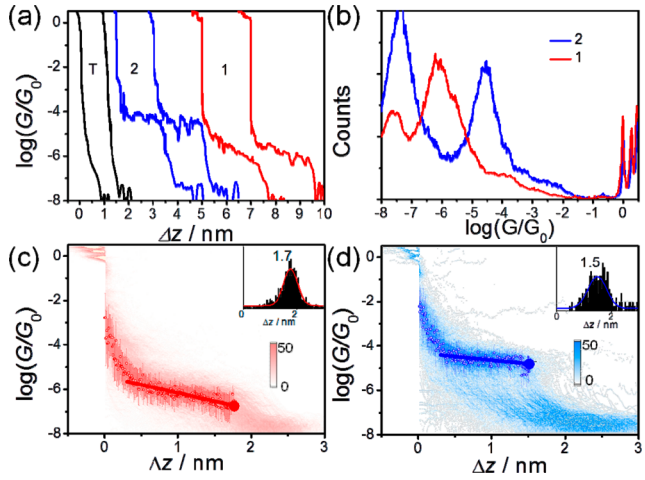

Figure 2. (a) Individual conductance−distance traces for **1** (red) and **2** (blue) using THF/mesitylene. (b) Conductance histograms for **1** (red) and **2** (blue). The sharp peak around $10^{-7.5}G_0$ is attributed to the noise limit of our MCBJ setup under the current experimental conditions. (c, d) 2D conductance histograms for (c) **1** and (d) **2**. In each histogram, statistically averaged conductance−distance traces (circles) with variations indicated by the standard deviations (bars) are shown, along with the linear fit (line).[44] The solid circle represents the last data point in the linear fit before junction rupture, and the solid error bar was determined from the Gaussian fit of the log G peak of the last data point.[44] Insets: Stretching distance distributions determined (c) from $0.1G_0$ to $10^{-7}G_0$ and (d) from $0.1G_0$ to $10^{-5.9}G_0$.

one-dimensional (1D) conductance histograms. As shown in Figure 2b, the most probable conductance for the anthanthrene molecules is $10^{-4.6}G_0$ for **2** and $10^{-6.1}G_0$ for **1**, indicating that the conductance of molecule **2** is a factor of 32 higher than the conductance of **1**. However, it should be noted that the most probable conductance results from the molecular conductances associated with different contact configurations and a variety of electrode separations. To facilitate comparison with theory, it is of interest to explore the molecular conductances through fully stretched junctions, for which contact occurs via the pyridyl groups. Quantitative analyses of 2D histograms (Figure 2c,d) reveal the evolution of molecular orientations and junction configurations during the stretching process.

The statistically averaged conductance−distance traces[44] (Figure 2c,d) exhibit "through-space" tunneling at the beginning of the stretching process (<0.3 nm) and then a clear molecular plateau with slightly different conductance decays for the two molecules. The analysis of stability and junction formation probability was performed by constructing the stretching distance distributions[44] shown in the insets of Figure 2c,d. The single-peak distribution suggests that the junction formation probability of the anthanthrene-based molecules could reach up to ∼100%. The single maximum in the plateau−length histogram represents the most probable relative characteristic stretching distance, Δz^* = 1.7 nm for **1** and 1.5 nm for **2**.

The most probable absolute displacement z^* in an experimental molecular junction formed between two gold tips is obtained by adding the snap-back distance (Δz_{corr}) to the relative displacement: $z^* = \Delta z^* + \Delta z_{corr}$. With $\Delta z_{corr} = 0.5 \pm 0.1$ nm, the z^* values are estimated to be 2.2 nm for **1** and 2.0 nm for **2**, which are quite close to the corresponding molecular lengths, suggesting that both molecules can be fully stretched during the break junction measurement. Thus, the con-

DOI: 10.1021/jacs.5b00335
J. Am. Chem. Soc. 2015, 137, 4469−4476

ductances of the fully stretched molecular junctions for molecules **1** and **2** are determined to be $10^{-6.7\pm0.7}G_0$ (solid red circle in Figure 2c) and $10^{-4.8\pm0.6}G_0$ (solid blue circle in Figure 2d), respectively, giving a conductance ratio of ~79, which is in good agreement with the MRR. To further investigate the accuracy of the MRR and to elucidate the origins of deviations from the rule, we performed DFT-based calculations of $T(E)$, the transmission coefficient for electrons of energy E to pass from one electrode to the other, from which the zero-temperature electrical conductance is given by the Landauer formula $G = G_0T(E_F)$ and the room-temperature conductance is obtained by integration over E of $T(E)$ weighted by the derivative of the Fermi function (see Computational Methods).

Clearly, the anthanthrene cores of molecules **1** and **2** do not directly contact the electrodes but instead make indirect contact via the pyridyl rings and acetylene linkers. Therefore, as an initial step, we computed the electrical conductances of anthanthrene cores in direct contact with the gold electrodes (Figure 3a). When the left and right electrodes are connected

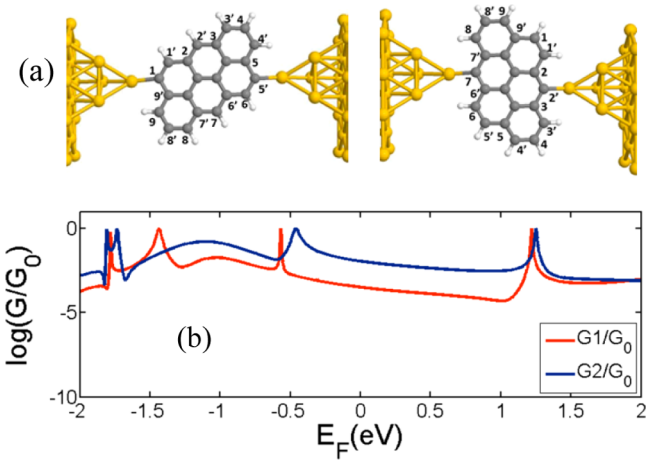

Figure 3. (a) Anthanthrene cores connected to gold electrodes via (left) the 1 and 5′ atoms and (right) the 7 and 2′ atoms. (b) Conductances of the anthanthrenes with 1,5′ (red curve) and 7,2′ (blue curve) cores obtained from DFT-NEGF calculations.

to atoms i,i' = 1,5′ respectively, this resembles the core of molecule **1**. Similarly, the structure connected via i,i' = 7,2′ resembles the core of molecule **2**. Figure 3b shows the conductances of the anthanthrenes with 1,5′ (red curve) and 7,2′ (blue curve) connectivities obtained from a DFT-NEGF calculation in the weak-coupling limit (when the gold−carbon distance is 2.4 Å). It is well-known that the value of the Fermi energy predicted by DFT (i.e., E_F^0 = 0 in Figure 3b) is not necessarily reliable, and therefore, it was of interest to evaluate the conductance ratio for various values of E_F. From Figure 3b we find that in the range 0.2 < E_F < 0.4 eV the conductance ratio varies between 69 and 88 and that a conductance ratio of 81 is obtained at E_F = 0.331 eV.

For the complete molecules measured experimentally, Figure 4c,d shows the logarithms of G/G_0 at zero and room temperature, respectively, for molecule **1** (red solid line) and **2** (blue solid line) as functions of the Fermi energy E_F. Since DFT does not yield the correct H−L gap, spectral adjustment has been employed on the basis of the experimental values of the H−L gaps.[47] As expected, Figure 4 shows that the value of the conductance ratio depends on the location of the Fermi energy, but whatever value is chosen within the H−L gap, the conductance of **2** is much greater than that of **1**, in agreement with the MRR trend. Indeed for a value of E_F = −0.33 eV, the conductance of molecule **2** ($10^{-4.98}$ G_0) is 81 times higher than that of molecule **1** ($10^{-6.9}$ G_0).

Beyond the molecules investigated above, we also examined conductance ratios of naphthalene and anthracene cores obtained from the experiments reported in ref 26. For naphthalene with 5,1′ and 3,5′ connectivities (molecules **4** and **6** in ref 26) conductances of 20.8 and 4.1 nS were reported, respectively, yielding a measured conductance ratio of 5.1. From Table 1, the MIs of these molecules are 2 and −1 respectively, yielding an MRR-predicted ratio of 4, which is in good agreement with the experimental ratio. For anthracene with 6,2′ and 4,7′ connectivities (molecules **5** and **7** in ref 26), conductances of 36.8 and 3.6 nS were reported, respectively, yielding a measured conductance ratio of 10.2. From the anthracene M-table presented in the SI, the MIs of these molecules are 4 and 1 respectively, yielding an MRR-predicted ratio of 16, which also captures the trend of the experimental ratio. In this case slight disagreements may arise because the conductance values in ref 26 include configurations in which contact is made directly with the core rather than only through the terminal anchor groups.

CONCLUSION

We have identified a new magic ratio rule (MRR) that captures the contribution of the connectivity to the conductance ratios of graphene-like cores when the coupling to the electrodes is weak and the Fermi energy coincides with the center of the HOMO−LUMO gap. The MRR is simple to implement and exact for a tight-binding bipartite lattice of identical sites with identical couplings when the Fermi energy is located at the gap center and the number of primed sites is equal to the number of unprimed sites. It states that the connectivity-driven conductance ratio is simply the square of the ratio of two "magic integers" whose values depend only on the connectivities to the electrodes. On the basis of their magic integers alone, the MRR predicts that the conductance of **2** is a factor of 81 higher than that of **1**, which is in good agreement with trends obtained from both experiment and DFT calculations. Literature values of conductances for naphthalene and anthracene[26] also reveal that the MRR predicts conductance trends for these molecules. This demonstrates that connectivity is a useful starting point for designing single-molecule junctions with desirable electrical properties. As an example of such design considerations, for the purpose of connecting molecules to a source or drain electrode, a high conductance is desirable. On the other hand, for the purpose of connecting to an electrostatic gate, a low conductance is needed to avoid leakage currents. Our study suggests that both features can be obtained using the same molecule provided the connectivities are selected with high and low MIs for source/drain and gate electrodes, respectively.

COMPUTATIONAL METHODS

DFT Calculations. The optimized geometry and ground-state Hamiltonian and overlap matrix elements of each structure were self-consistently obtained using the SIESTA[48] implementation of DFT. SIESTA employs norm-conserving pseudopotentials to account for the core electrons and linear combinations of atomic orbitals to construct the valence states. The generalized gradient approximation (GGA) of the exchange and correlation functional was used with the Perdew−

DOI: 10.1021/jacs.5b00335
J. Am. Chem. Soc. 2015, 137, 4469−4476

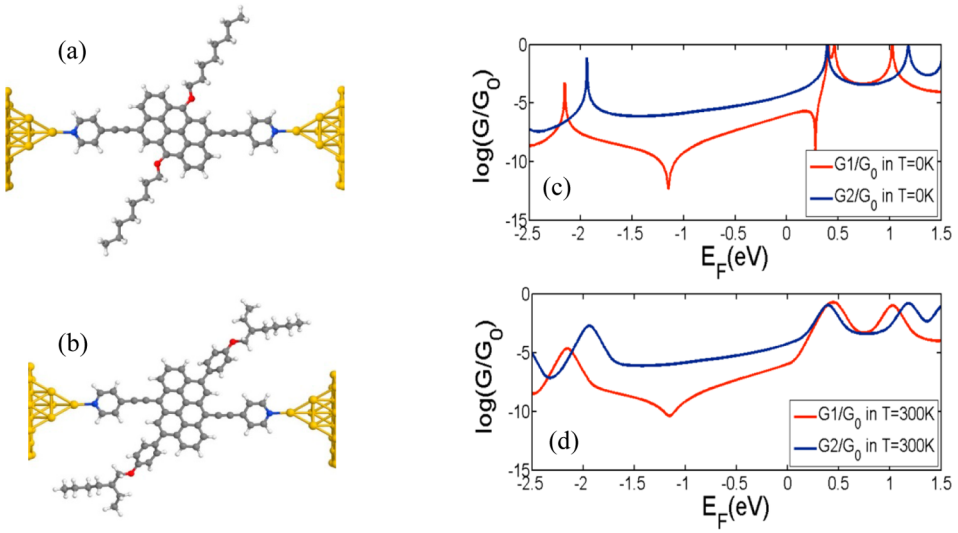

Figure 4. (a, b) Structures of (a) **1** and (b) **2** when the electrodes are connected to the nitrogen atoms of the pyridyl anchor groups. (c, d) Conductances of molecules **1** (red) and **2** (blue) at (c) zero temperature and (d) room temperature as functions of the predicted DFT gap from the Kohn–Sham mean-field Hamiltonian with spectral adjustments based on the experimental H–L gaps.

Burke–Ernzerhof parametrization (PBE)[49] a double-ζ polarized (DZP) basis set, and a real-space grid defined with an equivalent energy cutoff of 250 Ry. The geometry optimization for each structure was performed until the forces were smaller than 10 meV/Å.

Transport Calculations. The mean-field Hamiltonian obtained from the converged DFT calculation or a tight-binding Hamiltonian (using a single orbital energy site per atom with Hückel parametrization) was combined with our homemade implementation of the nonequilibrium Green's function method, GOLLUM,[50] to calculate the phase-coherent elastic scattering properties of each system, consisting of left (source) and right (drain) gold leads and the scattering region (molecule **1** or **2**). $T(E)$, the transmission coefficient for electrons of energy E to pass from the source to the drain, was calculated via the relation

$$T(E) = \mathrm{Tr}[\Gamma_R(E)G^R(E)\Gamma_L(E)G^{R\dagger}(E)]$$

in which $\Gamma_{L,R}(E) = i[\Sigma_{L,R}(E) - \Sigma^{\dagger}_{L,R}(E)]$ describes the level broadening due to the coupling between the left (L) or right (R) electrode and the central scattering region, $\Sigma_L(E)$ and $\Sigma_R(E)$ are the retarded self-energies associated with these couplings, and $G^R = (ES - H - \Sigma_L - \Sigma_R)^{-1}$ is the retarded Green's function, where H is the Hamiltonian and S is the overlap matrix. From the obtained transmission coefficient $T(E)$, the conductance was calculated using the Landauer formula $G = G_0 \int dE\, T(E)(-\partial f/\partial E)$, in which f is the Fermi function and $G_0 = 2e^2/h$ is the conductance quantum.

MATHEMATICAL METHODS

The following derivation of the MRR involves proving the three "ratio rules" given in eqs 1–3 stated below. Figure 5a shows an example of a structure of interest comprising a central region (2) connected by single atoms i and j to moieties on the left (1) and right (3). As noted in ref 31, the Green's function $\hat{G}_{ij}(E)$ connecting sites i and j of the structure in Figure 5a is proportional to the de Broglie wave amplitude at j created by an incoming electron at i, and the transmission coefficient $T_{ij}(E)$ is proportional to $|\hat{G}_{ij}(E)|^2$. Consequently, the ratio of the two transmission coefficients corresponding to connectivities i,j and l,m is given by the following generalized ratio rule (GRR):

$$T_{ij}(E)/T_{lm}(E) = |\hat{G}_{ij}(E)|^2/|\hat{G}_{lm}(E)|^2 \quad (1)$$

This ratio does not depend on details of the electrodes or anchor groups provided that these are identical for the two connectivities.

Furthermore, if the couplings to the moieties on the left and right are sufficiently weak and E does not coincide with an eigenvalue of the isolated central region 2, $\hat{G}_{ij}(E) \approx \hat{g}_{ij}(E)$, where $\hat{g}_{ij}(E)$ is the Green's function of the isolated central region. In this case, the ratio of the two transmission coefficients is given by the following weakly-coupled ratio rule (WRR):

$$T_{ij}(E)/T_{lm}(E) = |\hat{g}_{ij}(E)|^2/|\hat{g}_{lm}(E)|^2 \quad (2)$$

Finally, if E is located at the center of the H–L gap (i.e., if $E = E_F = 0$), then for a bipartite lattice of identical sites with equal numbers of primed and unprimed sites that is described by a tight-binding model, $\hat{g}_{ij}(0) \approx (-1/d)M_{ij}$. Hence, the ratio of the two transmission coefficients corresponding to connectivities i,j and l,m is given by the following magic ratio rule (MRR):

$$T_{ij}(0)/T_{lm}(0) = (M_{ij}/M_{lm})^2 \quad (3)$$

The derivation of these ratio rules starts with the observation that the structure in Figure 5a is mathematically equivalent to the three-component system in Figure 5b, in which the central region 2 is connected to components 1 and 3, which at large distances from 2 take

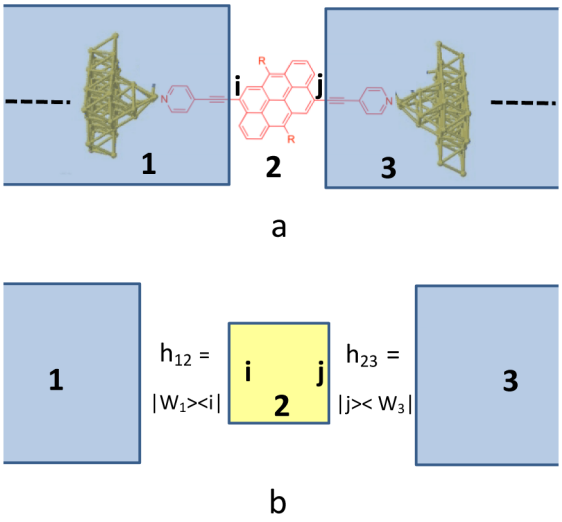

Figure 5. (a) Physical realization of a central moiety with sites i and j connected to current-carrying bonds that in turn are connected to anchor groups and external electrodes. (b) Mathematical abstraction of such a system, in which an "inner world" (2) is connected to an "outer world" (1 and 3) by coupling matrices h_{12} and h_{23}.

DOI: 10.1021/jacs.5b00335
J. Am. Chem. Soc. 2015, 137, 4469–4476

the form of crystalline periodic leads that extend to $-\infty$ and $+\infty$, respectively. Conceptually, when the coupling matrices h_{12} and h_{23} for coupling of 2 to these regions are set to zero, such a structure consists of a "closed inner world" (i.e., an inner vector space) 2, whose Green's function g_{22} (for real E) is Hermitian, connected to an open "outer world" composed of 1 and 3, whose Green's function is non-Hermitian.[51]

When the coupling matrices are nonzero, the transmission coefficient $T_{ij}(E)$ from 1 to 3 is obtained from the Green's function G_{31} connecting orbitals on electrode atoms of 1 to orbitals on electrode atoms of 3. In fact, at large distances from 2, where G_{31} can be projected onto scattering channels $|n_3\rangle$ and $|n_1\rangle$ of the crystalline leads of 3 and 1, the transmission coefficient can be written[51]

$$T_{ij}(E) = \sum_{n_1,n_3} T_{n_1n_3}(E) \tag{4}$$

where $T_{n_1n_3}(E) = V_{n_1}V_{n_3}|\langle n_3|G_{31}|n_1\rangle|^2$, in which V_{n1} and V_{n3} are the group velocities of electrons in channels $|n_1\rangle$ and $|n_3\rangle$. (As noted in ref 51, this expression is mathematically equivalent to the formula $T_{ij}(E) = 4\mathrm{Tr}\{\Gamma_1 G_{22}\Gamma_3 G_{22}^{\dagger}\}$, where G_{22} is the Green's function of region 2 in the presence of couplings to regions 1 and 3.)

When $h_{12} = 0$ and $h_{23} = 0$, we denote the Green's functions of components 1, 2, and 3 by g_{11}, g_{22}, and g_{33}, respectively. Then Dyson's equation yields

$$G_{31} = g_{33}h_{32}G_{22}h_{21}g_{11} \tag{5}$$

where

$$G_{22} = ({g_{22}}^{-1} - \Sigma)^{-1} \tag{6}$$

or equivalently

$$G_{22} = g_{22} + g_{22}\Sigma G_{22} \tag{7}$$

in which $\Sigma = \Sigma_1 + \Sigma_3$, where $\Sigma_1 = h_{21}g_{11}h_{12}$ and $\Sigma_3 = h_{23}g_{33}h_{32}$.

So far the analysis has been rather general. We now consider the case where 1 is coupled only to a single orbital $|i\rangle$ in 2 and 3 is coupled to only a single orbital $|j\rangle$ in 2. (More generally, $|i\rangle$ and $|j\rangle$ could be arbitrary vectors in the inner vector space.) This situation is described by coupling matrices of the form $h_{21} = |W_1\rangle\langle i|$ and $h_{32} = |W_3\rangle\langle j|$, where $|W_1\rangle$ ($|W_3\rangle$) is a vector of matrix elements in the space of 1 (3) describing the coupling of $|i\rangle$ ($|j\rangle$) to orbitals in 1 (3). In this case,

$$\Sigma = \sigma_1|i\rangle\langle i| + \sigma_3|j\rangle\langle j|$$

where

$$\sigma_l = \langle W_l|g_{ll}|W_l\rangle \qquad (l = 1 \text{ or } 3)$$

Writing

$$\hat{G}_{ij} = \langle i|G_{22}|j\rangle$$

$$\hat{g}_{ij} = \langle i|g_{22}|j\rangle$$

$$\hat{G} = \begin{pmatrix} \hat{G}_{ii} & \hat{G}_{ij} \\ \hat{G}_{ji} & \hat{G}_{jj} \end{pmatrix}$$

and

$$\hat{g} = \begin{pmatrix} \hat{g}_{ii} & \hat{g}_{ij} \\ \hat{g}_{ji} & \hat{g}_{jj} \end{pmatrix}$$

yields from eq 7

$$\hat{G} = \hat{g} + \hat{g}\sigma\hat{G} \tag{8}$$

where the self-energy matrix σ is given by

$$\sigma = \begin{pmatrix} \sigma_1 & 0 \\ 0 & \sigma_3 \end{pmatrix}$$

Hence

$$\hat{G} = \hat{g}(1 - \sigma\hat{g})^{-1} \tag{9}$$

Similarly, eq 5 yields

$$G_{31} = g_{33}|W_3\rangle\hat{G}_{ij}\langle W_1|g_{11} \tag{10}$$

This expression shows that all elements of the matrix G_{31} are proportional to the single number $\hat{G}_{ij}$. Hence, from eq 4,

$$T_{ij}(E) = L(E)|\hat{G}_{ij}|^2 \tag{11}$$

which proves the GRR of eq 1

In eq 11, the constant of proportionality $L(E) = \sum_{n_1,n_3} V_{n_1}V_{n_3}|\langle n_3|g_{33}|W_3\rangle\hat{G}_{ij}\langle W_1|g_{11}|n_1\rangle|^2$ is independent of the choice of i,j. Furthermore, in eq 9, $\hat{g}$ is independent of the couplings $|W_1\rangle$ and $|W_3\rangle$. On the other hand, the self-energies σ_1 and σ_3 do depend on the couplings and on i,j. However, these vanish in the weak-coupling limit, and therefore, for sufficiently weak couplings it is safe to neglect the product $\sigma\hat{g}$ in eq 9, provided that $\hat{g}$ is finite. Since $\hat{g}$ is the Green's function of the isolated region 2, which diverges when E coincides with an eigenvalue of 2, this condition requires that E should lie in an energy gap of 2. (It is interesting to note that this is the opposite of the condition for applicability of the Breit–Wigner formula for resonant transmission, which requires that E should be close to an energy level of 2.) When these conditions are satisfied, $\hat{G}_{ij}(E) \approx \hat{g}_{ij}(E)$, and the WRR of eq 2 is obtained. The WRR can be utilized by noting that $g_{22}(E) = (E - H)^{-1}$, where H is the Hamiltonian for the isolated region 2. The WRR is generally valid whenever $\sigma\hat{g}$ can be neglected compared with unity. Physically this means that if δ is the smaller of $|E_F - E_{HOMO}|$ and $|E_F - E_{LUMO}|$, then the level broadening Γ should be much less than δ (i.e., $\Gamma/\delta \ll 1$).

The MRR of eq 3 follows from the fact that if region 2 is a bipartite lattice, then the Hamiltonian H for the isolated region 2 is of the form

$$H = \begin{pmatrix} 0 & C \\ C^{\mathrm{t}} & 0 \end{pmatrix} \tag{12}$$

To obtain the transmission coefficient at the center of the HOMO–LUMO gap, we evaluate the associated Green's function at $E = 0$, which yields

$$g_{22}(0) = \left(-\frac{1}{d}\right)\begin{pmatrix} 0 & M^{\mathrm{t}} \\ M & 0 \end{pmatrix} \tag{13}$$

where d is the determinant of C and the matrix of MIs M is the transpose of the cofactor matrix of C. Since the ratio of two matrix elements of $g_{22}(0)$ does not involve d, this completes the derivation of the MRR of eq 3.

The condition that $g_{22}(0)$ is finite requires that d should not vanish. It is clear that $d = 0$ when the rows or columns of C are linearly dependent, which occurs when C is not a square matrix, i.e., when the number of primed sites is not equal to the number of unprimed sites. In this case, a transmission resonance occurs at $E = 0$, and the Breit–Wigner formula should be used. For this reason, the MRR is restricted to bipartite lattices of identical atoms with equal numbers of primed and unprimed atoms. If this condition is not satisfied, then for nonzero energies the WRR should be used.

Since the upper left (lower right) block of g_{22} corresponds to matrix elements between primed and primed (unprimed and unprimed) sites, the conductance vanishes when both electrodes are connected to primed sites only or unprimed sites only. For this reason, in addition to the nontrivial MIs shown in the M-tables, we assign an MI of zero to connectivities between primed and primed sites and between unprimed and unprimed sites.

The above derivation also reveals that in addition to the MIs, each lattice possesses a second integer d. To each magic integer $M_{ii'}$ we

DOI: 10.1021/jacs.5b00335
J. Am. Chem. Soc. 2015, 137, 4469–4476

assign a magic number (MN) defined by $m_{ii'} = M_{ii'}/d$. These MNs allow the prediction of conductance ratios of molecules with different central cores via a related MRR, which states that "the ratio of conductances of two molecules is equal to the square of the ratio of their magic numbers."

Finally, it is worth noting that knowledge of $T_{ij}(E)$ at $E = 0$ is particularly useful for bipartite lattices because $g_{22}(E)$ is symmetric about $E = 0$, so in the weak-coupling limit $T_{ij}(E)$ will have a maximum or minimum (depending on the sign of the MI) at $E = 0$. Therefore, at $E = 0$, $dT_{ij}(E)/dE = 0$ and $T_{ij}(E)$ varies slowly with E. Finally, we note that magic numbers are a useful concept for nonbipartite lattices of identical atoms provided that det H is nonzero. In this case, MIs are obtained by equating H to a connectivity matrix that contains unit matrix elements $H_{ij} = 1$ between connected sites i and j only and defining $M = (\det H)H^{-1}$. However, in this case the spectrum is not necessarily symmetric about the gap center and $T_{ij}(E)$ will not necessarily be either a maximum or a minimum at $E = 0$.

■ ASSOCIATED CONTENT

Supporting Information

Experimental procedures and additional computational data. This material is available free of charge via the Internet at http://pubs.acs.org.

■ AUTHOR INFORMATION

Corresponding Authors

*liu@dcb.unibe.ch
*c.lambert@lancaster.ac.uk
*hong@dcb.unibe.ch
*s.sangtarash@lancaster.ac.uk

Author Contributions

§Y.G., S.S., C.H., and H.S. contributed equally.

Notes

The authors declare no competing financial interest.

■ ACKNOWLEDGMENTS

This work was supported by the Swiss National Science Foundation (Grant 200021-147143), the European Commission (EC) FP7 ITN "MOLESCO" Project 606728, and the U.K. EPSRC (Grants EP/K001507/1, EP/J014753/1, and EP/H035818/1).

■ REFERENCES

(1) Chen, F.; Tao, N. *Acc. Chem. Res.* **2009**, *42*, 429.
(2) Pisula, W.; Feng, X.; Müllen, K. *Chem. Mater.* **2011**, *23*, 554.
(3) Carroll, R. L.; Gorman, C. B. *Angew. Chem., Int. Ed.* **2002**, *41*, 4378.
(4) Wu, J.; Pisula, W.; Müllen, K. *Chem. Rev.* **2007**, *107*, 718.
(5) Coskun, A.; Spruell, J. M.; Barin, G.; Dichtel, W. R.; Flood, A. H.; Botros, Y. Y.; Stoddart, J. F. *Chem. Soc. Rev.* **2012**, *41*, 4827.
(6) Zhang, L.; Fonari, A.; Liu, Y.; Hoyt, A.-L. M.; Lee, H.; Granger, D.; Parkin, S.; Russell, T. P.; Anthony, J. E.; Brédas, J.-L.; Coropceanu, V.; Briseno, A. L. *J. Am. Chem. Soc.* **2014**, *136*, 9248.
(7) Cai, J.; Ruffieux, P.; Jaafar, R.; Bieri, M.; Braun, T.; Blankenburg, S.; Muoth, M.; Seitsonen, A. P.; Saleh, M.; Feng, X. *Nature* **2010**, *466*, 470.
(8) Ruffieux, P.; Cai, J.; Plumb, N. C.; Patthey, L.; Prezzi, D.; Ferretti, A.; Molinari, E.; Feng, X.; Müllen, K.; Pignedoli, C. A. *ACS Nano* **2012**, *6*, 6930.
(9) Cai, J.; Pignedoli, C. A.; Talirz, L.; Ruffieux, P.; Söde, H.; Liang, L.; Meunier, V.; Berger, R.; Li, R.; Feng, X. *Nat. Nanotechnol.* **2014**, *9*, 896.
(10) Sedghi, G.; García-Suárez, V. M.; Esdaile, L. J.; Anderson, H. L.; Lambert, C. J.; Martín, S.; Bethell, D.; Higgins, S. J.; Elliott, M.; Bennett, N. *Nat. Nanotechnol.* **2011**, *6*, 517.
(11) Zhao, X.; Huang, C.; Gulcur, M.; Batsanov, A. S.; Baghernejad, M.; Hong, W.; Bryce, M. R.; Wandlowski, T. *Chem. Mater.* **2013**, *25*, 4340.
(12) Magoga, M.; Joachim, C. *Phys. Rev. B* **1999**, *59*, 16011.
(13) Papadopoulos, T.; Grace, I.; Lambert, C. *Phys. Rev. B* **2006**, *74*, No. 193306.
(14) Wang, C.; Bryce, M. R.; Gigon, J.; Ashwell, G. J.; Grace, I.; Lambert, C. J. *J. Org. Chem.* **2008**, *73*, 4810.
(15) Ke, S.-H.; Yang, W.; Baranger, H. U. *Nano Lett.* **2008**, *8*, 3257.
(16) Finch, C.; Garcia-Suarez, V.; Lambert, C. *Phys. Rev. B* **2009**, *79*, No. 033405.
(17) Bergfield, J. P.; Solis, M. A.; Stafford, C. A. *ACS Nano* **2010**, *4*, 5314.
(18) Ricks, A. B.; Solomon, G. C.; Colvin, M. T.; Scott, A. M.; Chen, K.; Ratner, M. A.; Wasielewski, M. R. *J. Am. Chem. Soc.* **2010**, *132*, 15427.
(19) Markussen, T.; Schiötz, J.; Thygesen, K. S. *J. Chem. Phys.* **2010**, *132*, No. 224104.
(20) Solomon, G. C.; Bergfield, J. P.; Stafford, C. A.; Ratner, M. A. *Beilstein J. Nanotechnol.* **2011**, *2*, 862.
(21) Sadeghi, H.; Mol, J. A.; Lau, C. S.; Briggs, G. A. D.; Warner, J.; Lambert, C. J. *Proc. Natl. Acad. Sci. U.S.A.* **2015**, *112*, 2658.
(22) Hong, W.; Valkenier, H.; Mészáros, G.; Manrique, D. Z.; Mishchenko, A.; Putz, A.; García, P. M.; Lambert, C. J.; Hummelen, J. C.; Wandlowski, T. *Beilstein J. Nanotechnol.* **2011**, *2*, 699.
(23) Vazquez, H.; Skouta, R.; Schneebeli, S.; Kamenetska, M.; Breslow, R.; Venkataraman, L.; Hybertsen, M. *Nat. Nanotechnol.* **2012**, *7*, 663.
(24) Ballmann, S.; Härtle, R.; Coto, P. B.; Elbing, M.; Mayor, M.; Bryce, M. R.; Thoss, M.; Weber, H. B. *Phys. Rev. Lett.* **2012**, *109*, No. 056801.
(25) Aradhya, S. V.; Meisner, J. S.; Krikorian, M.; Ahn, S.; Parameswaran, R.; Steigerwald, M. L.; Nuckolls, C.; Venkataraman, L. *Nano Lett.* **2012**, *12*, 1643.
(26) Kaliginedi, V.; Moreno-García, P.; Valkenier, H.; Hong, W.; García-Suárez, V. M.; Buiter, P.; Otten, J. L.; Hummelen, J. C.; Lambert, C. J.; Wandlowski, T. *J. Am. Chem. Soc.* **2012**, *134*, 5262.
(27) Aradhya, S. V.; Venkataraman, L. *Nat. Nanotechnol.* **2013**, *8*, 399.
(28) Arroyo, C. R.; Tarkuc, S.; Frisenda, R.; Seldenthuis, J. S.; Woerde, C. H.; Eelkema, R.; Grozema, F. C.; van der Zant, H. S. *Angew. Chem., Int. Ed.* **2013**, *125*, 3234.
(29) Guédon, C. M.; Valkenier, H.; Markussen, T.; Thygesen, K. S.; Hummelen, J. C.; van der Molen, S. J. *Nat. Nanotechnol.* **2012**, *7*, 305.
(30) Prins, F.; Barreiro, A.; Ruitenberg, J. W.; Seldenthuis, J. S.; Aliaga-Alcalde, N.; Vandersypen, L. M.; van der Zant, H. S. *Nano Lett.* **2011**, *11*, 4607.
(31) Ashwell, G. J.; Urasinska, B.; Wang, C.; Bryce, M. R.; Grace, I.; Lambert, C. J. *Chem. Commun.* **2006**, 4706.
(32) Lambert, C. *Chem. Soc. Rev.* **2015**, *44*, 875.
(33) Yoshizawa, K.; Tada, T.; Staykov, A. *J. Am. Chem. Soc.* **2008**, *130*, 9406.
(34) Yoshizawa, K. *Acc. Chem. Res.* **2012**, *45*, 1612.
(35) Fowler, P.; Pickup, B.; Todorova, T.; Myrvold, W. *J. Chem. Phys.* **2009**, *131*, No. 244110.
(36) Fowler, P.; Pickup, B.; Todorova, T.; Myrvold, W. *J. Chem. Phys.* **2009**, *131*, No. 044104.
(37) Mayou, D.; Zhou, Y.; Ernzerhof, M. *J. Phys. Chem. C* **2013**, *117*, 7870.
(38) Markussen, T.; Stadler, R.; Thygesen, K. S. *Nano Lett.* **2010**, *10*, 4260.
(39) Winzenberg, K. N.; Kemppinen, P.; Fanchini, G.; Bown, M.; Collis, G. E.; Forsyth, C. M.; Hegedus, K.; Singh, T. B.; Watkins, S. E. *Chem. Mater.* **2009**, *21*, 5701.
(40) Burke, K. B.; Shu, Y.; Kemppinen, P.; Singh, B.; Bown, M.; Liaw, I. I.; Williamson, R. M.; Thomsen, L.; Dastoor, P.; Belcher, W. *Cryst. Growth Des.* **2012**, *12*, 725.
(41) Cardia, R.; Malloci, G.; Mattoni, A.; Cappellini, G. *J. Phys. Chem. A* **2014**, *118*, 5170.

DOI: 10.1021/jacs.5b00335
J. Am. Chem. Soc. 2015, 137, 4469−4476

(42) Giguère, J.-B.; Boismenu-Lavoie, J.; Morin, J.-F. *J. Org. Chem.* **2014**, *79*, 2404.
(43) Maliakal, A.; Raghavachari, K.; Katz, H.; Chandross, E.; Siegrist, T. *Chem. Mater.* **2004**, *16*, 4980.
(44) Fudickar, W.; Linker, T. *J. Am. Chem. Soc.* **2012**, *134*, 15071.
(45) Hong, W.; Manrique, D. Z.; Moreno-Garcia, P.; Gulcur, M.; Mishchenko, A.; Lambert, C. J.; Bryce, M. R.; Wandlowski, T. *J. Am. Chem. Soc.* **2012**, *134*, 2292.
(46) Hong, W.; Li, H.; Liu, S.-X.; Fu, Y.; Li, J.; Kaliginedi, V.; Decurtins, S.; Wandlowski, T. *J. Am. Chem. Soc.* **2012**, *134*, 19425.
(47) García-Suárez, V. M.; Lambert, C. J. *New J. Phys.* **2011**, *13*, No. 053026.
(48) Soler, J. M.; Artacho, E.; Gale, J. D.; García, A.; Junquera, J.; Ordejón, P.; Sánchez-Portal, D. *J. Phys.: Condens. Matter* **2002**, *14*, 2745.
(49) Perdew, J. P.; Burke, K.; Ernzerhof, M. *Phys. Rev. Lett.* **1996**, *77*, 3865.
(50) Ferrer, J.; Lambert, C.; García-Suárez, V.; Manrique, D. Z.; Visontai, D.; Oroszlany, L.; Rodríguez-Ferradás, R.; Grace, I.; Bailey, S.; Gillemot, K.; Sadeghi, H.; Algharagholy, L. A. *New J. Phys.* **2014**, *16*, No. 093029.
(51) Claughton, N. R.; Leadbeater, M.; Lambert, C. J. *J. Phys.: Condens. Matter* **1995**, *7*, 8757.

DOI: 10.1021/jacs.5b00335
J. Am. Chem. Soc. 2015, 137, 4469−4476